N O T I C E

THIS DOCUMENT HAS BEEN REPRODUCED FROM MICROFICHE. ALTHOUGH IT IS RECOGNIZED THAT CERTAIN PORTIONS ARE ILLEGIBLE, IT IS BEING RELEASED IN THE INTEREST OF MAKING AVAILABLE AS MUCH INFORMATION AS POSSIBLE

NASA Technical Memorandum 81482
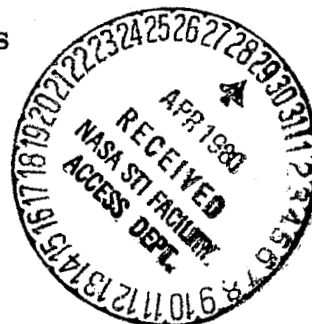
HIGH SPEED TURBOPROPS FOR
EXECUTIVE AIRCRAFT - POTENTIAL
AND RECENT TEST RESULTS

Daniel C. Mikkelson and Glenn A. Mitchell
Lewis Research Center
Cleveland, Ohio

HIGH SPEED TURBOPROPS FOR EXECUTIVE AIRCRAFT -
POTENTIAL AND RECENT TEST RESULTS

By

Daniel C. Mikkelson, Head
Subsonic Propulsion Section

and

Glenn A. Mitchell
Aerospace Engineer

National Aeronautics and Space Administration
Lewis Research Center
Cleveland, Ohio

ABSTRACT

Turboprop powered executive aircraft are currently operating at
cruise Mach numbers up to about Mach 0.5, and future aircraft may
extend this speed to near Mach 0.8. These aircraft generally offer
relatively low energy consumption characteristics. Studies by NASA
and industry indicate that at higher speeds (Mach 0.7 to 0.8) block
fuel savings from 15 to near 40% may be possible with advanced turbo-
prop propulsion relative to comparable turbofan powered aircraft. These
large potential savings result from the high inherent propulsive
efficiency of the free air propeller. Achieving that potential requires
reducing propeller compressibility losses through several advanced
aerodynamic concepts.

To evaluate the potential of advanced propeller technology, four high
speed propeller models were designed and tested in the Lewis Research
Center 8x6 foot wind tunnel. Results from these tests show that the
combination of: increased blade number, aerodynamically integrated pro-
peller/nacelles, reduced blade thickness, spinner area ruling, and blade
sweep were important in achieving high propeller efficiency at these high
cruise speeds. Several advanced propeller analytical programs are under
development to insure that future propeller designs will be both more
efficient and offer a lower acoustic environment.

INTRODUCTION

The requirement for improved energy conservation from all modes of
transportation is a vital need of the United States and free world
countries. As an important part of this transportation system,
executive air travel will have to achieve improvements in the use of
energy in both the near and far terms. Advanced turboprop propulsion
for executive aircraft that cruise in the Mach 0.6 to 0.8 speed range,
has the potential for some significant advantages compared to turbo-
fan powered aircraft. In addition to a large energy savings potential,
advanced turboprop propulsion has the potential for improved low speed
aircraft performance with reduced airport community noise while achieving
reduced aircraft total operating cost.

ADVANCED TURBOPROP POTENTIAL

The high cruise speed (Mach 0.6 to 0.8) and "over-the-weather" high
altitude capability of current turbofan powered executive aircraft,
along with airline de-regulation, are some of the key reasons that this
segment of the business aircraft industry has shown significant growth
in the past year. To offer a viable alternative to this type of pro-
pulsion, an advanced high speed turboprop will have to offer similar
performance and ride quality. Current propeller powered business air-
craft are limited to maximum cruise speeds near Mach 0.5 due to the size
of existing turboshaft engines and the fall-off in propeller efficiency
above this speed for current technology general aviation propellers.
These twin-engine aircraft are powered by reciprocating and turboshaft
engines in the 150 to 750 kilowatt (200 to 1000 horsepower) size and
have maximum cruise speeds that range from about Mach 0.3 to 0.5 as
shown in figure 1. Higher cruise speeds may be possible with future
improvements in the technology of turboshaft engines and propellers.
Several new engines in the 1040 to 1490 kilowatt (1400 to 2000 horse-
power) range are under development for future commuter aircraft and
NASA and industry are currently studying the potential of further advances
in turboprop propulsion for this category of aircraft (reference 1 and 2).
This advanced engine technology may have direct application to future
high performance executive aircraft. In addition, propeller technology
for both low and high speed aircraft is being advanced through the research
currently underway as part of NASA's Advanced Turboprop Project and pro-
peller base R&T program. Recent summaries of this work are given in
references 3 and 4.

A model of an advanced high speed turboprop aircraft and its unique
propulsion system is shown in figures 2 and 3, respectively. This air-
craft includes a number of advanced airframe and propulsion system con-
cepts. A high aspect ratio wing that incorporated winglets and advanced
supercritical airfoils is shown along with a "T-tail" empenage configura-
tion (for minimizing any potentially adverse slipstream interaction).
The advanced propeller would be powered by a modern turboshaft engine
and gear box to provide the maximum power to the propeller with a minimum

engine fuel consumption. Propeller efficiency would be kept high by minimizing or eliminating compressibility losses. This would be accomplished by utilizing thin swept blades that would be integrally designed with an area ruled spinner and nacelle. Blade sweep would also be used to reduce noise during both take-off/landing and during high speed cruise flight. Aircraft operations at high altitudes and Mach 0.6 to 0.8 requires much higher power than used on current propeller aircraft. A power loading (shaft horsepower divided by propeller diameter squared) about 5 times higher than current business turboprops would be needed to minimize propeller diameter and weight. Eight or ten blades are required to increase ideal efficiency at these higher disk loadings. In addition to these advanced concepts, a modern blade fabrication technique is needed to construct the thin, highly swept and twisted blades.

The installed efficiency that is projected for the advanced high speed turboprop compared to current low speed turboprops and high bypass ratio turbofans is shown in figure 4 over a range of cruise speeds. Installation losses that are accounted for in the data of this figure include: nacelle drag for the turboprop systems; and fan cowling external drag and the internal fan airflow losses associated with inlet recovery and nozzle efficiency for the turbofan systems. Current technology turboprops have a level of installed efficiency that is slightly over 80 percent at cruise speeds up to Mach 0.5. Above this speed, efficiency falls off significantly due to large propeller compressibility losses. These current turboprops generally incorporate general aviation propellers that use blades with thickness to chord ratios (at 75 percent radius) that range from 5 to 7 percent. These rather thick blades are the main cause of low efficiency at Mach numbers above 0.5.

The advanced high speed turboprop has the potential for delaying these compressibility losses to much higher cruise speeds. With this propulsion system, performance can remain high to at least Mach 0.8 cruise. At Mach 0.8 the installed efficiency of turbofan systems would be approximately 65 percent compared to about 75 percent for the advanced turboprop. This large performance advantage may offer some attractive energy savings for future high performance executive aircraft.

A number of studies have been conducted by both NASA and industry to evaluate the potential of advanced high speed turboprop propulsion for both civil and military applications. Numerous references to specific studies and summary results are listed in reference 5. The trip fuel savings trend shown in figure 5 plotted versus operating range is a summary of these studies. Installed efficiency levels similar to those shown in figure 4 for comparable technology advanced turboprops and turbofans were used in most of these studies. As shown in figure 5, trip fuel savings is dependent on aircraft cruise speed and range. At the bottom of the band, associated with Mach 0.8 cruise, fuel savings

3

range from about 15 to 30 percent for advanced turboprop aircraft compared to equivalent technology turbofan aircraft. The larger fuel savings occurs at the shorter operating ranges where the mission is climb and descent dominated. Because of the lower operating speeds encountered during climb and descent, turboprops have an even larger performance advantage than the advantage at Mach 0.8 cruise conditions. In a similar manner, a larger fuel savings is possible at Mach 0.7 cruise (represented by the top of the band in figure 5). At this lower cruise speed fuel savings range from about 25 to near 40 percent.

The advantages of an advanced turboprop powered executive aircraft over a comparable turbofan technology aircraft were examined in a mission analysis for an 8 passenger, 1700 nautical mile executive aircraft. Details of the assumed aircraft can be found in the appendix. NASA's General Aviation Synthesis Program (GASP) (ref. 6) was used to calculate the aircraft performances for cruise speeds of Mach 0.6 and 0.7 and cruise altitudes of 7.6, 10.7, and 13.7 kilometers (25, 35, and 45 thousand feet). The aircraft were resized for each cruise speed and altitude. Figure 6 presents the trip fuel savings for an advanced turboprop compared to a comparable high bypass ratio turbofan over the range of cruise altitudes that were studied. The fuel savings potential calculated for the executive turboprop at Mach 0.7 range from 19 to 25 percent with the largest savings occuring for the 35,000 foot aircraft. For the Mach 0.6 turboprop the fuel savings potential was about 5 percent larger.

A comparison of total operating cost (TOC) for the advanced turboprop and turbofan executive aircraft is shown in figure 7. The TOC equation that was used in the GASP program can be found in the appendix, and includes total costs over a 5 year period with a 500 hour per year utilization rate. Results are presented for both Mach 0.6 and 0.7 cruise speeds for fuel costs that vary from $1 to $5 per gallon. With a fuel cost of one dollar per gallon the total operating cost of the turboprop powered aircraft ranges from 79 to 82 percent of the operating cost of a turbofan aircraft for cruise Mach numbers of 0.6 and 0.7 respectively. At a fuel cost of $5 per gallon the relative operating cost of the turboprop decreases to only 75 and 78 percent of the turbofan level for the same speeds. For the Mach 0.7 design turboprop, the five year projected TOC saving over a comparable turbofan ranges from about $140,000 to $320,000 as fuel prices increase from $1 to $5 per gallon.

ADVANCED DESIGN CONCEPTS

The high efficiency shown in figure 4 for the advanced high speed turbprop can be achieved by aerodynamically designing to minimize compressibility losses. Some of these design concepts are shown in figure 8. In the blade tip region compressibility losses are reduced by using thin airfoil sections and by sweeping the blade tips, as illustrated by the two sketches at the top of the figure. Sweep

4

is also an effective means of reducing propeller noise as some later figures will show. In the hub region, the blockage of the nacelle behind the propeller, and an area ruled spinner are used to reduce compressibility losses. These concepts are illustrated by the next two sketches in figure 8. Advanced airfoil technology for high performance and low noise signature have not yet been applied to high speed turboprop designs but may provide future improvements. Since all of these advanced concepts are interrelated, an integrated procedure is used to design high speed propellers and nacelles (references 5 and 7). Some advanced aerodynamic analysis programs are currently being developed to better model the complicated propeller/nacelle flow field. This work is described in reference 8.

The effects of applying these advanced concepts to a propeller design are shown in figure 9. This figure is based on a cruise condition of Mach 0.8 and shows the propeller blade Mach number as it varies from hub to tip. The local blade Mach number includes both the free stream component and the rotational component, and is represented by curve A. At the hub the local Mach number is slightly higher than the cruise speed of Mach 0.8. As the rotational velocity component becomes larger at increased radius, the relative Mach number increases until it reaches Mach 1.14 at the blade tip. This Mach number must be compared to the drag rise Mach number of each blade airfoil section to evaluate the propeller performance potential. The predicted drag rise Mach number (Figure 4, Curve B) was obtained from isolated two-dimensional airfoil data for a high-speed propeller having thickness-to-chord ratios of about 15 percent at the hub and 2 percent at the blade tip. Across the entire blade radius the local Mach number (Curve A) is higher than the drag rise Mach number (Curve B). This represents a potentially large compressibility loss.

The advanced aerodynamic concepts shown in figure 8 are effective in minimizing or eliminating these losses. In the outer portions of the propeller, the blades are swept to reduce the component of velocity normal to the blade airfoil section, similar to swept wing theory. With a sufficient amount of sweep the local Mach number (Curve A) can be reduced to an effective Mach number (Curve C) that is below the drag rise Mach number (Curve B) in the outer portions of the blade. This procedure significantly reduces the compressibility losses in the blade tip region and can also be effective in reducing noise. In the hub region, the spinner-nacelle body is tailored to increase the effective nacelle blockage behind the propeller and reduce the local Mach number through the propeller plane. This effect is shown by the local surface Mach number distribution plotted in figure 9 and the resulting effective section Mach number of Curve D. Near the hub the effective section Mach number is suppressed far below the drag rise Mach number. With a large number of blades (8 in this example), the hub blade sections operate as a cascade and the additional Mach number suppression is necessary to prevent blade-to-blade choking. Area ruling the spinner between the blades gives further protection from choking by opening the flow area between the blades at the spinner.

5

PROPELLER MODEL DESIGNS

In a cooperative program between NASA-Lewis Research Center and
Hamilton Standard the concepts described above were used to design
a series of propeller models for wind tunnel testing. The three
basic blade planforms pictured in figure 10 represent the four pro-
peller designs. All of the propellers have a blade tip speed of 244
m/sec (800 ft/sec), cruise power loading of 301 kW/m^2 (37.5 hp/ft^2)
and 8 blades. The planforms are identified by sweeps of 0, 30°
and 45°. Here the tip sweep is approximately the angle of the tip
of the blade measured back from a radial line normal to the axis
of rotation.

The straight blade and one of the 30° swept blades (SR-1) were
initial designs using established analyses (reference 8) that lacks
a refined methodology to design the twist of a swept blade. Initial
tests of the 30° swept design (SR-1) indicated a retwist was required
(which was actually a redistribution of the blade load from hub to
tip). That became the second 30° swept design (SR-1M). The 45°
swept blade (SR-3) was designed for acoustic suppression as well
as improved aerodynamic performance by tailoring the sweep and plan-
form shape. More detailed discussions of the aero/acoustic design
methodology are presented in references 4, 9 and 10.

The efficiency and noise level that were predicted at the time these
blades were designed are listed in figure 10 and indicate improved
performance with increased sweep. The noise predictions indicated
some reduction for 30° of sweep and significant reduction for the
aero/acoustic 45° swept design.

The photographs in figure 11 show the 0°, 30°, and 45°, swept, 62.2
cm (24.5 in) diameter propeller models installed on the Propeller
Test Rig (PTR) in the NASA-Lewis 8-by-6 foot wind tunnel. The
tunnel (ref 11) has a porous wall test section to minimize any
wall interactions. The PTR is powered by a 746 kW (1000 hp) air
turbine using a continous flow 3.1 X 10^6 N/m^2 (450 psi) air system
routed through the support strut. Axial force and torque on the
propeller are measured on a rotating balance located inside of an
axisymmetric nacelle behind the propeller.

PROPELLER AERODYNAMIC PERFORMANCE

Typical test results from the 45° swept design are shown in figure 12.
The data are presented in the conventional propeller performance
plot format. Net thrust efficiency and a dimensionless power
coefficient are plotted as ordinates. The abscissa is advance ratio
which is proportional to the ratio of flight or advance speed to
blade tip speed. As tip speed increases from windmill (no power),
the advance ratio decreases as shown by the two horizontal scales.

6

Blade angle is set and data are taken from windmill to higher power shown by the data symbols on the power coefficient plot. The blade angle (β 3/4), measured at 3/4 of the propeller radius, becomes 90° when the chord of that airfoil section is aligned directly with the flight direction. As power is increased the thrust increases and, as seen in the upper data curves, the net thrust efficiency increases. reaches a peak, and then begins to drop off. All blade angles yield similar power and efficiency curves.

Power loading (P/D^2) can be written in terms of propeller coefficients and free-stream conditions as:

$$\frac{P}{D^2} \equiv \frac{C_p}{J^3} \; (\rho_o V_o^3)$$

From this relationship a line of constant power loading has been added to Fig. 12 and represents the design loading parameter C_p/J^3 (= 0.05933) corresponding to P/D^2 = 301 kW/m^2 (37.5 hp/ ft^2) as determined at the design operating condition of J = 3.06 and C_p = 1.7. This line represents the design power at different propeller tip speeds. The efficiency at the design power can be found for each blade angle, indicated by each vertical dot-dash line. Then the variation of net efficiency with advance ratio (i.e., tip speed) at design power can be plotted as shown in figure 13. This plot is for models with area-ruled spinners, at the design power loading at Mach 0.8. Curves of net efficiency versus advance ratio are compared for different sweep angles. Significant improvement can be seen in going from 0° to 30° of sweep. The 45° swept blade shows still more improvement, especially at low values of advance ratio corresponding to high tip speeds. The overall improvement at the design advance ratio of 3.06 is about 3 percent.

Other important design variations were investigated using the 30° swept designs. As noted in the description of the blade designs, there were two different twist or loading distributions with the same 30° swept planform. The blade design with the revised (reduced) twist was tested with both a conic and an area-ruled spinner. The performance comparison of these variations is shown in figure 14; again at the design Mach number and power loading. The original 30° swept propeller design (baseline twist) was tested only with a conic spinner. The performance of this configuration is represented by the lowest of the three data curves in figure 14. Retwisting the blade to increase the load at the tip improved the performance at all but the lower advance ratios. Peak performance was obtained at the design advance ratio of 3.06. The retwisted design was also tested with an area-ruled spinner. That change improved the performance about 1 percent over the full range of tip speeds tested. Thus, the proper twist to obtain a more optimum loading and the technique of area-ruling to alleviate near-hub compressibility problems are important factors in obtaining high propeller performance at cruise speeds near Mach 0.8.

7

Figures 13 and 14 have shown propeller performance at the design power loading and Mach number. Similar plots at other free-stream Mach numbers can then yield propeller net efficiency at the design power coefficient and advance ratio for other cruise speeds. Figure 15 was generated in this manner and shows net efficiency versus Mach number for the 0°, 30°, and 45° swept blade designs with area-ruled spinners. Because the power coefficient and advance ratio are constant in this figure, the ideal efficiency is also constant as is shown by the upper dashed line. The ideal efficiency represents the performance of an optimumally loaded propeller with no blade drag. The gap in figure 15 between the ideal efficiency line and the experimental performance curves represents the viscous and compressibility losses. As the data curves show, those losses increase at the higher speeds due to increasing compressibility losses. However, the performance of the 45° swept blade decreased a smaller amount with increasing speed than the performance of propellers with less sweep. At Mach 0.85 the 45° swept blade achieved a 4% performance gain over the straight blade. The gain at Mach 0.8 was about 3% as previously shown in figure 13. At the lower speeds of Mach 0.6 to 0.7 both swept blades had approximately a 2 to 3 percent efficiency advantage over the straight blade and the highest performing design had an efficiency that exceeded 81 percent. The study level (shown on figure 15) of 79.5 percent efficiency at Mach 0.8, was the value used in projecting the large fuel efficiency and operating cost advantages of an advanced turboprop over an equivalent technology turbofan powered aircraft. The 45° swept propeller at this speed had an efficiency of 78.7% which was close to this study level.

By operating the 45° swept propeller at off design lower power loadings higher efficiencies can be obtained at Mach 0.8. This is shown in figure 16 where net efficiency is plotted against advance ratio for several levels of power loading. The typical variation of efficiency with advance ratio at a constant power loading is a peaked curve. The reduction from the peak with increasing advance ratio is due to a combination of lower ideal efficiencies due to increased swirl and lower blade sectional lift to drag ratios (from increasing local angles of attack). The fall-off with decreasing advance ratio is due to increased compressibility losses associated with the higher tip rotational speeds and/or again lower blade sectional lift to drag ratios (from decreasing local angles of attack).

The effect of operating the propeller at reduced power loading was an improvement in efficiency. At 80 percent design power loading an efficiency near 80 percent was obtained at an advance ratio of 3.3. This power loading would result in a 12 percent larger propeller diameter; however, propeller noise would probably be lower due to the decreased tip speed. In an actual aircraft installation, the lower noise and increased performance must be balanced against

8

the increased propeller size which can affect the overall airplane design and may cause increased weight and cost penalties. The increased performance may more than make up for this penalty, but this will depend on the specific application. A thorough airplane mission analysis study would be required to determine the desirability of modifying the propeller "design point" to optimize the overall aircraft performance. Additional propeller performance details from the wind tunnel tests are given in reference 5.

PROPELLER ACOUSTIC PERFORMANCE

In order for an advanced turboprop aircraft to be competitive with an advanced turbofan aircraft, the turboprop cabin interior during cruise should be equivalent in comfort (low levels of noise and vibration) to that of the turbofan aircraft. A quiet cabin interior will be more difficult to achieve in the turboprop aircraft. This is because its fuselage may be in the direct noise field of the propeller whereas the inlet duct of a turbofan shields the fuselage from fan noise. Advanced technologies are being applied to reducing propeller source noise and improving fuselage wall noise attenuation to meet the turbofan cabin comfort levels. Lockheed and Bolt Beranek and Newman study results have shown improved wall attenuation potential for reduced weight penalty by using a double wall fuselage construction and lighter composite materials (references 12 and 13). Reduced propeller source noise is being studied with propeller sweep and new acoustic analysis techniques.

In addition to the performance data shown earlier, acoustic measurements were made in the Lewis 8-by-6 foot wind tunnel on the high-speed turboprop models. The noise data were obtained from pressure transducers located on the side-wall and ceiling of the tunnel. Though the porous-walled tunnel does not have acoustic damping material on any of its walls and absolute noise levels may be subject to question because of reflections, the relative acoustic data obtained indicated that information about the noise differences among the propellers was usable. Details of these acoustic tests are presented in reference 5, and additional high-speed propeller acoustic results are presented in references 14 and 15.

The wave shapes of the measured near-field pressure generated by the blades operating near the design conditions are shown in figure 17. These are pressure-time traces for both the straight blade and the aero/acoustically designed 45° swept blade. They were obtained from the transducer on the tunnel wall nearest to the propeller plane. The straight blade propeller produced a high amplitude, steep wave shape which approached the classic N wave shock pattern. However, the quieter 45° swept blade produced an almost sinusoidal wave which was also of considerably less amplitude. These differences in the character of the noise indicate that the aero/acoustically designed planform of the 45° swept blade was successful in reducing the sharp pressure rise that would normally be associated with supersonic helical tip speed propellers.

9

The magnitude of the noise reduction achieved with the 45° swept propeller is more apparent in figure 18. The maximum blade passage tone measured on the tunnel ceiling is plotted against the helical tip (total, including flight and rotational) Mach number. The data were obtained at approximately the design power coefficient and advance ratio, and the helical tip Mach number was varied by changing tunnel and propeller rotational speed. In general, the noise of both the straight and 45° swept blade increased rapidly as the helical tip speed approached Mach 1.0. At higher helical tip speeds the noise level was approximately constant. Over the complete test range, the noise level of the 45° swept blade was consistently lower than that of the straight blade. At the design tip Mach number it was 5 to 6 dB lower. At lower Mach numbers the noise reduction was slightly larger (7 to 9 dB).

This noise reduction at the design point agrees well with the predicted value shown in figure 10, and indicates that by utilizing advanced acoustic analysis programs to properly sweep high speed propellers it is possible to achieve significant noise reductions.

TEST SUMMARY

The noise reductions discussed above and the high performance that was measured show that there are attractive aerodynamic and acoustic benefits from the advanced concepts that were investigated in the recent NASA propeller tests. High aerodynamic performance was obtained at Mach 0.8. At this speed, the highest performing propeller (45° sweep) had an efficiency of 78.7% which was within about 1 percent of the study value used to predict a large potential fuel savings for advanced high speed turboprops. Efficiency near 80 percent was obtained at a power loading only 20 percent lower than the design value. At speeds in the Mach 0.6 to 0.7 range the highest performing design had an efficiency that exceeded 81 percent at the design C_p and J. Nacelle blockage was an important design concept, and spinner area ruling increased efficiency about 1 percent. Blade tip sweep improved efficiency about 3 percent and reduced cruise noise about 6 dB at Mach 0.8 for the 45° swept model that was based on an aero/acoustic design approach.

FUTURE PERFORMANCE POTENTIAL

The performance results achieved with the recent high speed propeller tests show that an advanced turboprop may be an attractive energy efficient alternative for future high speed executive aircraft. In addition, further efficiency improvements and noise reductions may be possible with some of the advanced experimental and analytical technology work that is underway or planned as part of NASA's high speed propeller research program. Figure 19 indicates the future of high speed turboprop improvements. The efficiency envelope for

the recent tunnel tests shows that performance near 80 percent was possible for models that were designed using established analyses and several advanced concepts. Three future models are currently being designed or are planned for design. These models will include such features as: 10 bladed designs, enhanced tip sweep and lower tip speeds to improve acoustic as well as aerodynamic performance. Both refined analysis methods, which are currently available, and some more advanced analysis methods, which are under development, will be used in the design of these models. The more advanced methods will be used as they become available for the designs planned further in the future. It is anticipated that these future models will be about 2 percent higher in performance than the models that were recently tested. Another approach which is being studied to further improve performance is to recover the thrust lost in the swirl of the propeller slipstream. This loss for highly loaded propellers can be as much as 6 to 8 percent. Methods being considered for swirl recovery are coaxial counter-rotation, wing contouring, and the introduction of stators behind the propeller.

The advanced aerodynamic analysis methods that are bing developed to better model the complicated flow field of high speed propellers are shown in figure 20. Both lifting line and lifting surface representations of the propeller blades are under development and a summary of these analyses is given in reference 8. Most current business aircraft propellers are designed based on the established lifting line analyses of Goldstein (reference 16) and Theodorsen (reference 17). These analyses cannot properly account for blade sweep, the influence of the spinner and nacelle, and the mixed subsonic and supersonic flow over the blades. Because of these limitations two advanced lifting line analyses are being developed. A curved lifting line analysis has been developed by Sullivan (reference 18) which removes some of these limitations. This analysis can presently analyze blades of any planform in the presence of a cylindrical nacelle. The other lifting line analysis handles the propeller and nacelle in an interactive approach (reference 19). With this analysis, the propeller wake flow conforms to the nacelle shape. In addition, supersonic tip speed corrections are included that modify the induced velocity that is calculated in this region, and also three-dimensional Mach cone corrections are made to the airfoil data used with the analysis.

Since the blades of advanced high speed propellers will have relatively low aspect ratios, lifting surface analyses should give a much closer representation of the actual blade flow field. Two analytical programs are planned for this area. A solution to the three-dimensional Euler equations for propeller flow fields is under development. These equations describe the flow of an inviscid compressible fluid and can accurately determine the losses due to shock waves. A simplified approach is obtained when losses due to shock waves are neglected. This approach solves the transonic potential equation in three dimensions and gives both better flow field resolution and faster computing time. An effort in this area is planned for the future.

11

SYMBOLS

C_p power coefficient = $P/\rho_o n^3 D^5$

D blade tip diameter, cm(in.)

dB decibel

J advance ratio, V_o/nD

M Mach number

M_ℓ local Mach number

M_o free-stream Mach number

n rotational speed, revolutions per second

P power, kW (hp)

R blade tip radius, cm (in.)

r radius, cm (in.)

SPL sound pressure level, dB

SR single rotation

T_{net} thrust, newtons (lb)

$(TOC)_{TP}$ total operating cost, turboprop

$(TOC)_{TF}$ total operating cost, turbofan

V_o free-stream velocity, m/sec (ft/sec)

V_{TIP} blade rotational tip velocity, m/sec (ft/sec)

X axial distance, cm (in.)

$\beta\ 3/4$ blade angle at 75% radius, deg

η_{net} net efficiency = $(T_{net} \cdot \dot{V}_o)/P$

ρ_o free-stream density, kg/m^3 (slugs/ft^3)

REFERENCES

1. D. J. Giulianetti and L. J. Williams, "Toward New Small Transports for Commuter Airlines," Astronautics & Aeronautics, Vol. 18, February 1980, pp. 16-25.

2. T. L. Galloway, "Small Transport Aircraft Technology," Astronautics & Aeronautics, Vol. 18, February 1980, pp. 26-35.

3. D. C. Mikkelson, "NASA Propeller Technology Program," General Aviation Propulsion, NASA CP 2126, 1980, pp. 315-325.

4. J. F. Dugan, Jr., B. S. Gatzen, and W. M. Adamson, "Prop-Fan Propulsion- Its Status and Potential," SAE paper 780995, SAE Aerospace Meeting, San Diego, Calif., November 27-30, 1978.

5. R. J. Jeracki, D. C. Mikkelson, and B. J. Blaha, "Wind Tunnel Performance of Four Energy Efficient Propellers Designed for Mach 0.8 Cruise," NASA TM-79124 or SAE Paper 790573, April 1979.

6. "GASP - General Aviation Synthesis Program, Volume 1 - Main, Volume 2 - Geometry, Volume 3 - Aerodynamics, Volume 4 - Propulsion, Volume 5 - Economics, Volume 6 - Mission Analysis, Volume 7 - Weight and Balance," Aerophysics Research Corporation, Report No. NASA CR-152303 on Contract No. NAS2-9352, January 1978.

7. D. C. Mikkelson, B. J. Blaha, G. A. Mitchell, and J. E. Wikete, "Design and Performance of Energy Efficient Propellers for Mach 0.8 Cruise," NASA TM X-73612 or SAE Paper 770458, March 1977.

8. L. J. Bober, and G. A. Mitchell, "Summary of Advanced Methods for Predicting High Speed Propeller Performance," NASA TM X-81409 or AIAA Paper 80-0225, January 1980.

9. F. B. Metzger and C. Rohrback, "Aero-Acoustic Design of the Prop-Fan," AIAA Paper 79-0610, AIAA 5th Aero-Acoustics Conference, Seattle, Washington, March 1979.

10. D. B. Hanson, "Near Field Noise of High Tip Speed Propellers in Forward Flight," AIAA Paper 76-565, AIAA 3rd Aero-Acoustics Conference, Palo Alto, July 1976.

11. R. J. Swallow and R. A. Aiello, "NASA Lewis 8- by 6- Foot Supersonic Wind Tunnel," NASA TM X-71542, 1974.

12. J. D. Revell, F. J. Balena, and L. R. Koval, "Analytical Study of Interior Noise Control by Fuselage Design Techniques on High Speed Propeller - Driven Aircraft," Lockheed-California Company, Burbank, CA, Report No. NASA CR-15922, on Contract No. NAS1-15427, 1980.

13. D. C. Rennison, J. F. Wilby, and A. H. Marsh, "Interior Noise Control Prediction Study for High-Speed Propeller-Driven Aircraft," Bolt Beranek and Newman, Inc., Canoga Park, CA, Report No. NASA CR-159200, On Contract No. NAS1, 15426, 1980.

14. J. H. Dittmar, B. J. Blaha, and R. J. Jeracki, "Tone Noise of Three Supersonic Helical Tip Speed Propellers in a Wind Tunnel at 0.8 Mach Number," NASA TM-79046, 1978.

15. J. H. Dittmar, R. J. Jeracki, and B. J. Blaha," Tone Noise of Three Supersonic Helical Tip Speed Propellers in a Wind Tunnel," NASA TM-79167, 1979.

16. S. Goldstein, "On the Vortex Theory of Screw Propellers," Royal Society (London) Proceedings, Vol. 123, No. 792, Apr. 6, 1929, pp. 440-465.

17. T. Theodorsen, "Theory of Propellers," New York, NY: McGraw-Hill, 1948.

18. J. P. Sullivan, "The Effect of Blade Sweep on Propeller Performance," AIAA Paper 77-716, June 1977.

19. T. A. Egolf, O. L. Anderson, D. E. Edwards, and A. J. Landgrebe, "An Analysis for High Speed Propeller-Nacelle Aerodynamic Performance Prediction, Volume 1, Theory and Initial Application and Volume 2, User's Manual for the Computer Program," United Technologies Research Center, East Hartford, CT, Report No. R79-912949-19, June 1979.

Appendix - Executive Aircraft and Total Operating Cost
Definition

The 8 passenger (including crew) executive aircraft that were
studied with the General Aviation Synthesis Program (GASP) had a
7120 newton (1600 pound) design payload over a 3150 kilometer
(1700 nautical mile) range. A constant wing loading of 2870
N/m^2 (60 lbs./ft.^{2}) and aspect ratio 10 wing with full span Fowler
flaps was used to provide a relatively short runway capability with
good low speed performance. Advanced airframe technology was assumed
by reducing the empty weight and zero lift drag by 15 percent over
current technology levels for both the turboprop and turbofan
powered aircraft. Comparable levels of advanced technology were
used with both propulsion systems. Maximum turbine inlet temperature
of 1520^{0}K (2100^{0}F) was used. The turbofans had bypass ratios of
about 5; and the turboprops used cruise propeller efficiencies of
85 and 83 percent for Mach 0.6 and 0.7, respectively. The advanced
turboprop was penalized for a 1 percent gross weight increase due
to additional fuselage acoustic attenuation weight. Also, the
turboprop acquisition costs were scaled up to better reflect the
anticipated higher costs of the advanced propellers.

The total operating cost (TOC) over a five year period of ownership
was determined from the following equation:

$$TOC = AC + OC + I - RV$$

WHERE:

AC = <u>Acquistion Cost</u> is the total retail price of the aircraft

OC = <u>Operating Cost</u> is based on 500 hr/yr utilization and includes
fuel, oil, inspection and maintenance, overhaul
reserve, insurance, storage and FAA tax

I = <u>Interest</u> is based on a 5 year loan with a 20% down payment and
a 10% interest rate

RV = <u>Resale Value</u> is assumed to be 70% of acquisition cost

15
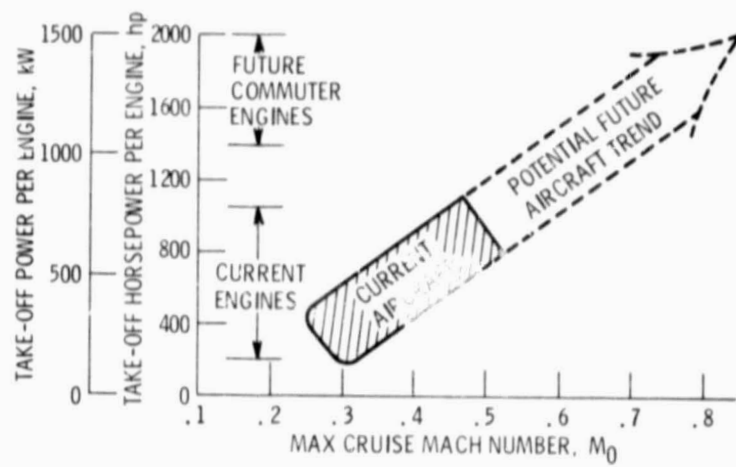
Figure 1. - Executive aircraft cruise Mach number trend.

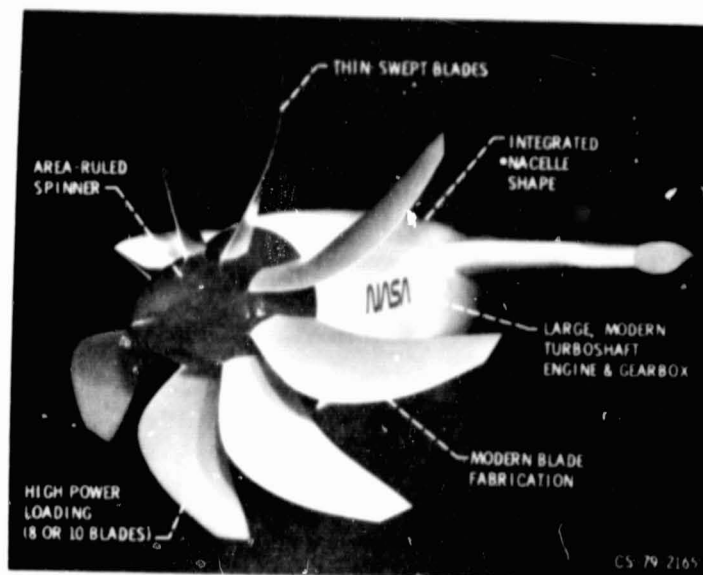Figure 2. - High speed executive turboprop aircraft.
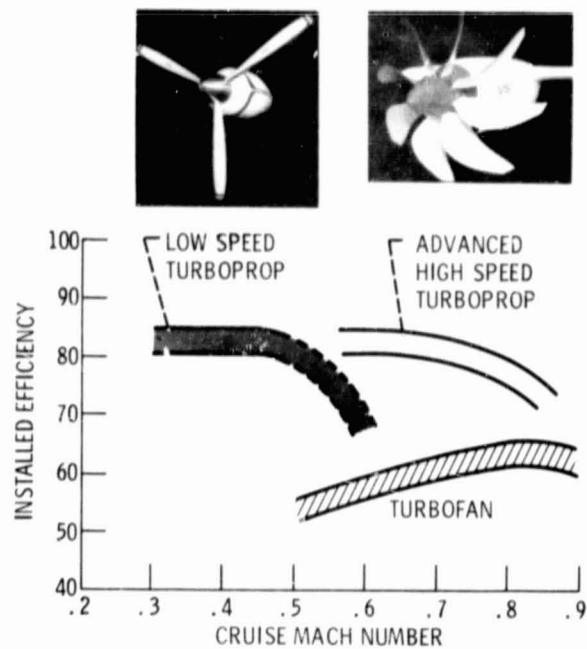
Figure 3. - Advanced turboprop propulsion system.
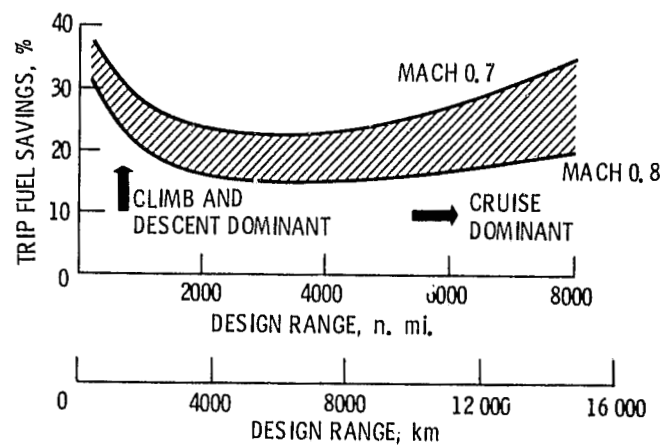

Figure 4. - Installed cruise efficiency trends.

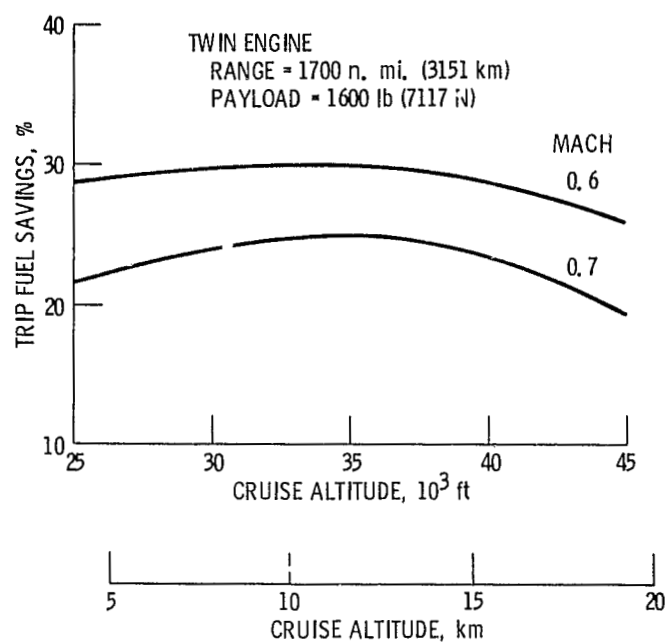Figure 5. – Fuel savings trends of advanced turboprop aircraft over comparable turbofan aircraft.

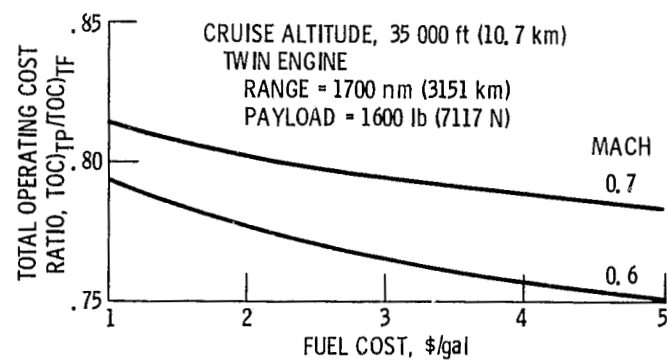Figure 6. – Effect of design cruise altitude on executive aircraft fuel savings. Advanced turboprop over comparable turbofan.

Figure 7. – Effect of fuel price on the ratio of turboprop to turbofan total operating cost.

REDUCED THICKNESS

BLADE SWEEP

NACELLE BLOCKAGE

SPINNER AREA RULING

ADVANCED AIRFOILS
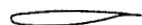
Figure 8. – Advanced aerodynamic concepts for improving high speed propeller performance.

CS-79-1472

CURVE

A	SECTION MACH NUMBER, NO VELOCITY SUPPRESSION OR SWEEP
B	DRAG DIVERGENCE MACH NUMBER (NACA 16-SERIES)
C	SECTION MACH NUMBER WITH 30^0 TIP SWEEP
D	EFFECTIVE SECTION MACH NUMBER (WITH SUPPRESSION AND SWEEP)

$M_0 = 0.8$, 243.8 m/sec (800 ft/sec) TIP SPEED 8 BLADES, 10.668 km (35 000 ft) ALTITUDE
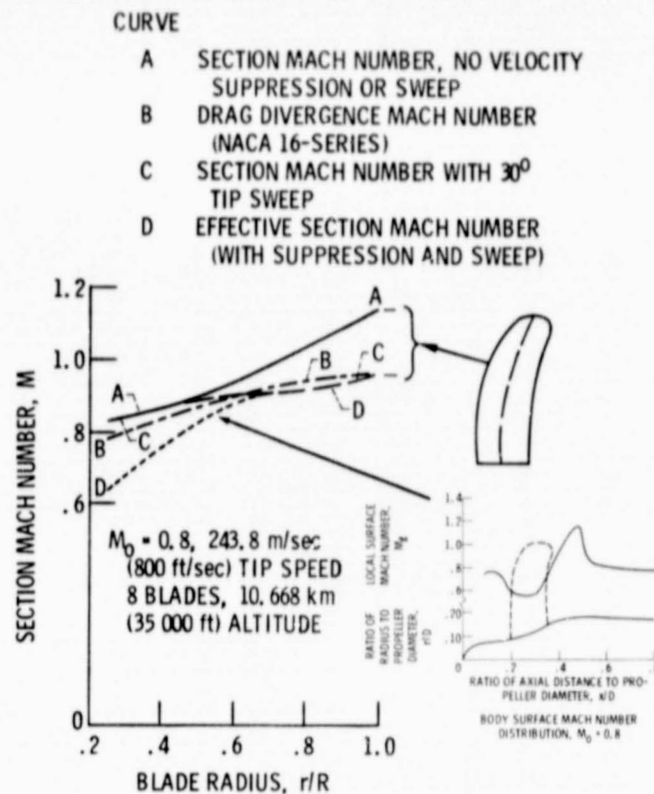
Figure 9. - Effects of advanced aerodynamic concepts on blade section Mach number distributions.

	SR-2	SR-1, 1M	SR-3
TIP SWEEP ANGLE, deg	0	30	45
PREDICTED DESIGN EFF, %	76.6	78.9, 79.3	81.1
PREDICTED DESIGN NOISE REDUCTION, Δ dB	REF.	-2	-6

TIP SPEED, ft/sec (m/sec)	800 (244)
POWER LOADING, P/D^2, hp/ft^2 (kW/m^2)	37.5 (301)
NO. OF BLADES	8

CS-79-4176
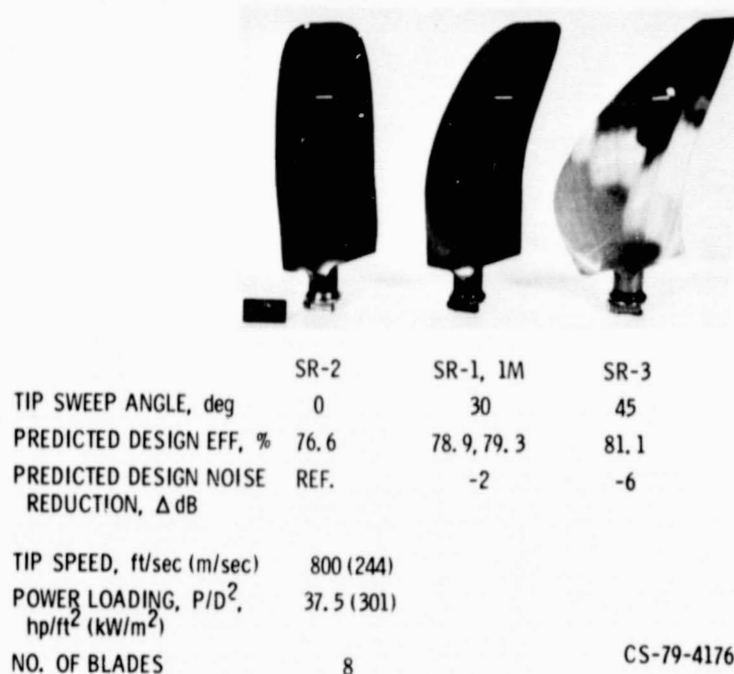
Figure 10. - Design characteristics and planforms of high speed propeller models.

30° SWEEP

0° SWEEP

45° SWEEP

CS-79-871
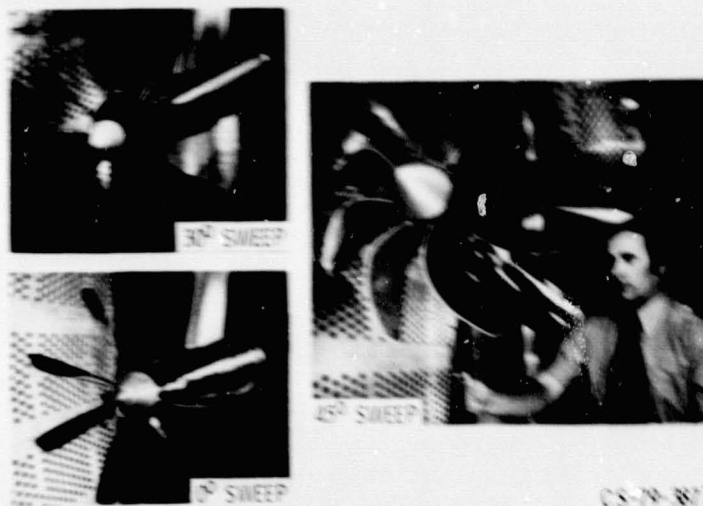
Figure 11. - Installation of propeller models in Lewis 8- by 6-Foot Wind Tunnel.

$M_0 = 0.8$

DESIGN POWER LOADING

$\beta_{3/4}$

64.7°

60.3°

NET EFF, η NET

POWER COEFF, c_p

ADVANCE RATIO, J

V_{TIP}, ft/sec (35 000 ft ALTITUDE)

V_{TIP}, m/sec (10.7 km ALTITUDE)
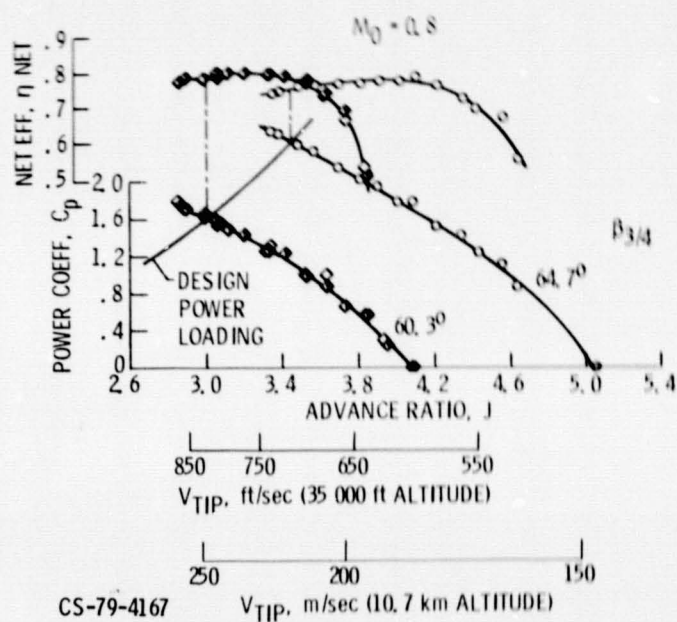
CS-79-4167

Figure 12. - Basic measured performance for SR-3, 45° swept propeller.
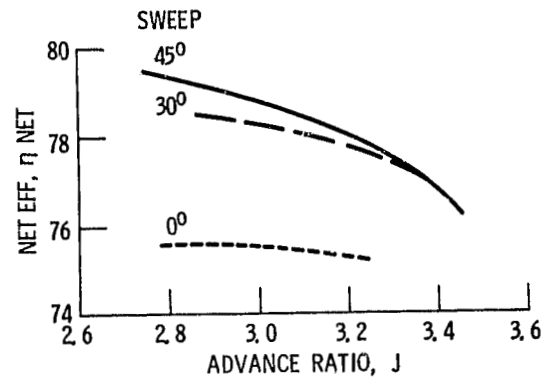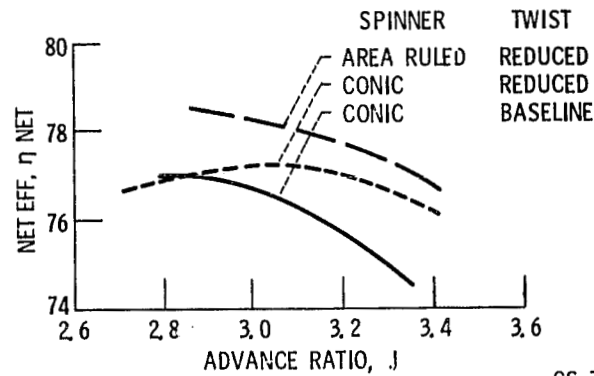
AREA RULED; MACH 0.8; 100% DESIGN POWER LOADING

Figure 13. - Effect of blade sweep on measured
net efficiency.

CS-79-4168

30° SWEEP; MACH 0.8; 100% DESIGN POWER

CS-79-4172

Figure 14. - Effect of twist and area ruling on
net efficiency.

AREA RULED SPINNER, J =3.06, C_p = 1.7
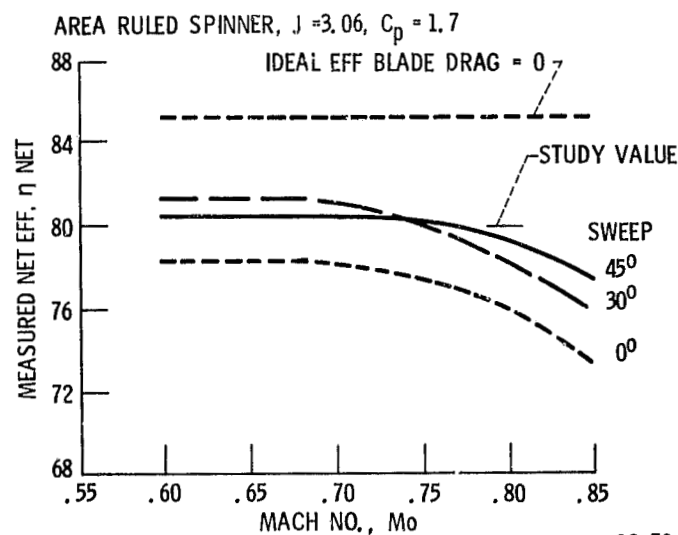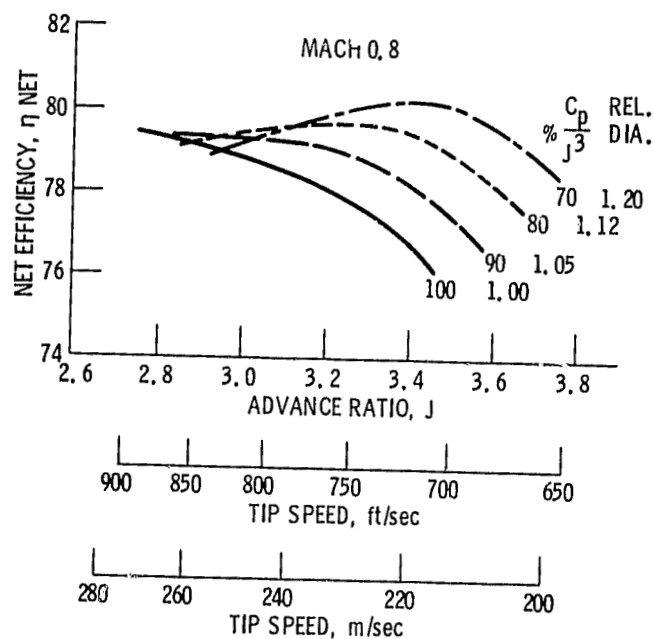

CS-79-4173

Figure 15. - High speed propeller performance
summary.

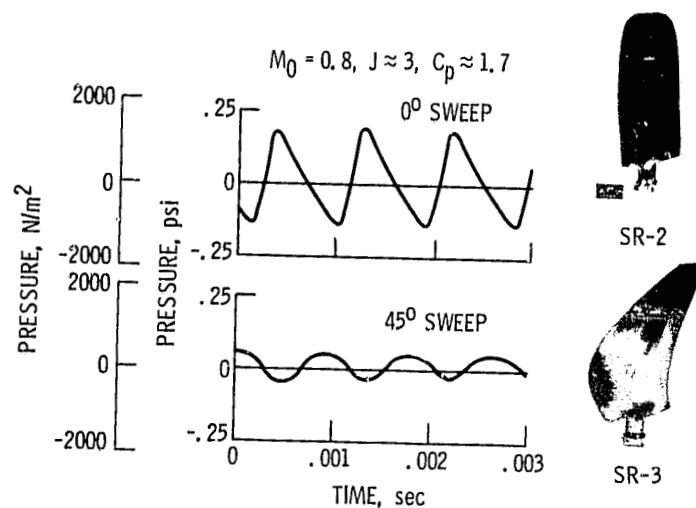Figure 16. – Effect of power loading and advance ratio on performance of the SR-3, 45° swept propeller.

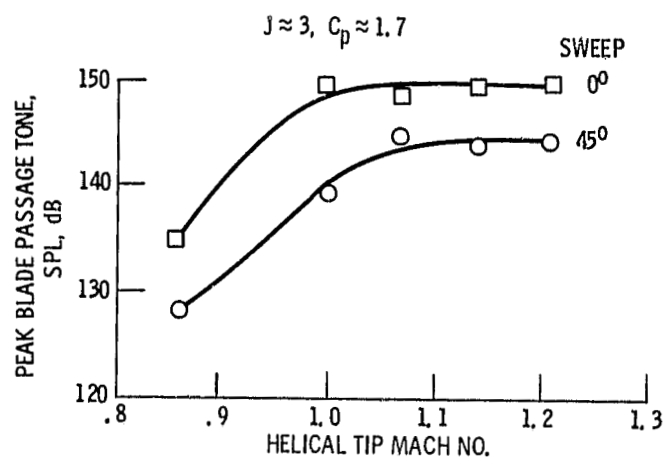Figure 17. – Effect of sweep on measured near field acoustic pressure signature.

$J \approx 3,\ C_p \approx 1.7$

Figure 18. – Effect of tip Mach number on measured near field noise.
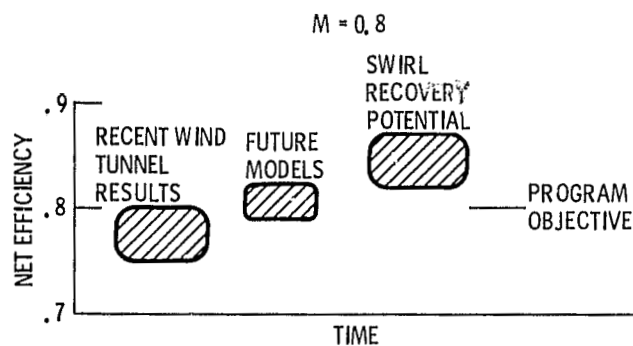
$M = 0.8$

Figure 19. – Summary of high speed propeller performance potential.

LIFTING LINE POTENTIAL ANALYSES
  ESTABLISHED APPROACH
  CURVED LIFTING LINE ANALYSIS
  PROPELLER NACELLE INTERACTION ANALYSIS

3-D COMPRESSIBLE LIFTING SURFACE ANALYSES
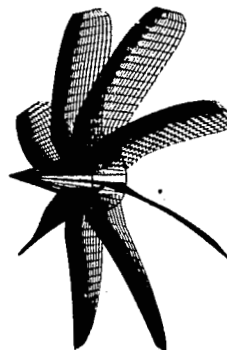 EULER EQUATIONS
  TRANSONIC POTENTIAL EQUATION

Figure 20. – Advanced analysis methods for improving propeller performance.